Available online at www.sciencedirect.com

ScienceDirect

Mendeleev Commun., 2024, **34**, 481–483

Mendeleev Communications

Stabilization of the perovskite phase of $CsPbI_3$ with isonipecotic acid

Nadezhda N. Dremova,[a] Gennady V. Shilov,[a] Pavel A. Troshin[b,a] and Lyubov A. Frolova*[a]

[a] *Federal Research Center of Problems of Chemical Physics and Medicinal Chemistry, Russian Academy of Sciences, 142432 Chernogolovka, Moscow Region, Russian Federation. E-mail: lyuanfro@gmail.com*
[b] *Zhengzhou Research Institute, Harbin Institute of Technology, Zhengzhou, Henan Province, 450000 China*

DOI: 10.1016/j.mencom.2024.06.004

To significantly improve phase photostability, $CsPbI_3$ absorber films were modified by introducing isonipecotic acid. This has resulted in remarkable long-term operational stability of $CsPbI_3$-based perovskite solar cells with optimally modified light absorbers.

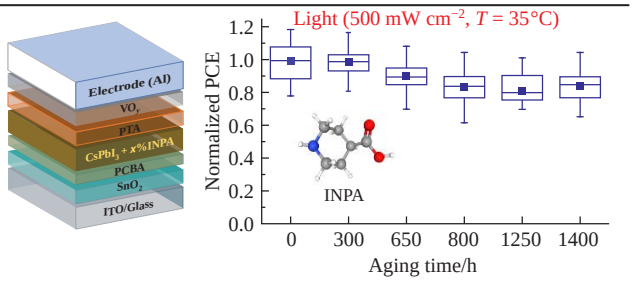

Keywords: perovskite solar cells, cesium lead triiodide, phase stability, stabilizing agent, photostability, defect passivation, long-term stability.

Hybrid perovskite solar cells based on complex lead halides have gained considerable interest due to the feasibility of their low-cost production and the ability to achieve impressive power conversion efficiencies exceeding 26%, approaching those of silicon solar cells.[1–3] However, the main obstacle to their practical implementation is the poor operational stability of hybrid perovskites with organic cations.[4–6] $CsPbI_3$-based perovskite solar cells have become the focus of attention due to their excellent thermal stability and acceptable bandgap.[7–9] $CsPbI_3$ does not decompose irreversibly into its constituent salts under the influence of moisture, elevated temperatures and exposure to light, as is observed for hybrid perovskites with organic cations. In addition, theoretical calculations show that the maximum power conversion efficiency (PCE) of $CsPbI_3$ solar cells can reach 21.7%.[10] However, the photoactive black polymorphic phases of $CsPbI_3$ such as cubic (α), tetragonal (β) and orthorhombic (γ) are thermodynamically unstable and undergo phase transformation to the unwanted non-photoactive yellow δ-$CsPbI_3$ phase.[11] Moreover, the poor phase stability of $CsPbI_3$ leads to a high density of defects at the surface and grain boundaries in perovskite films, in particular, under-coordinated Pb^{2+} ions and surface charged defects, which further accelerate the photodegradation of the perovskite phase. The formation of the unwanted yellow δ-$CsPbI_3$ phase is significantly accelerated by exposure to light, moisture and air.

An effective way to increase the thermodynamic stability of the dark phase of $CsPbI_3$ and suppress phase transitions is to introduce various organic compounds into perovskite films. Certain modifiers can be incorporated into the three-dimensional structure of $CsPbI_3$ perovskite to form quasi-2D perovskites with reduced dimensionality, suppressing phase transitions due to thermodynamic limitations.[12–15] Other modifying agents are typically localized on the surface of perovskite grains and passivate defects at the grain boundaries. For example, organic additives such as amines or sulfides containing functional groups with a lone pair of electrons are able to bind to the Pb^{2+} cation and thus passivate defects on the surface of the perovskite film.[16] Another approach to increasing phase stability is to reduce the size of perovskite crystals down to nanometers through the use of organic additives that suppress crystal growth during the formation of perovskite films. For example, amino acids are used as ligands to passivate surface defects of $CsPbI_3$.[17]

Using this strategy, a wide variety of organic compounds such as organic ammonium salts, amino acids, π-conjugated polymers and others have been investigated as stabilizing components for $CsPbI_3$.[17–24] However, most studies have examined the effect of modification of the $CsPbI_3$ absorber on the stability of films or solar cells with respect to environmental humidity.[24,25]

In this work, we modified $CsPbI_3$ absorber films by introducing isonipecotic acid (INPA) to significantly improve their phase photostability and also to ensure the long-term stability of $CsPbI_3$-based perovskite solar cells containing optimally modified light absorbers.

$CsPbI_3$ films with different INPA [Figure 1(*a*)] contents from 0 to 30 mol% were deposited by a one-step spin-coating method from a 0.625 M precursor solution containing equimolar amounts of CsI and PbI_2 dissolved in *N*,*N*′-dimethylformamide–dimethyl sulfoxide (7 : 1) followed by annealing at 140 °C (for details, see Online Supplementary Materials).

To reveal the effect of INPA on the lattice parameters of $CsPbI_3$ films, we performed X-ray diffraction (XRD) measurements. According to Figure 1(*b*), in the case of the pristine $CsPbI_3$ film, the main diffraction peaks corresponding to the yellow orthorhombic phase δ-$CsPbI_3$ (space group *Pnma*) and the peaks of the dark perovskite phase γ-$CsPbI_3$ (space group *Pnam*) were detected at 2θ of approximately 14, 20, 29 and 41°.[26,27] All INPA-modified films exhibited diffraction peaks corresponding only to the pure γ-$CsPbI_3$ perovskite structure without any impurity phases [see Figure 1(*b*)]. Films modified with 5% INPA show higher diffraction peak intensities suggesting improved crystallinity of $CsPbI_3$ [see Figure 1(*b*)]. A further increase in the INPA concentration leads to a decrease in the intensity of the XRD peaks, which indicates a decrease in the crystallinity of the absorber films.

The UV-VIS absorption spectra of the resulting thin films with different INPA contents are shown in Figure 1(*c*). Low-energy

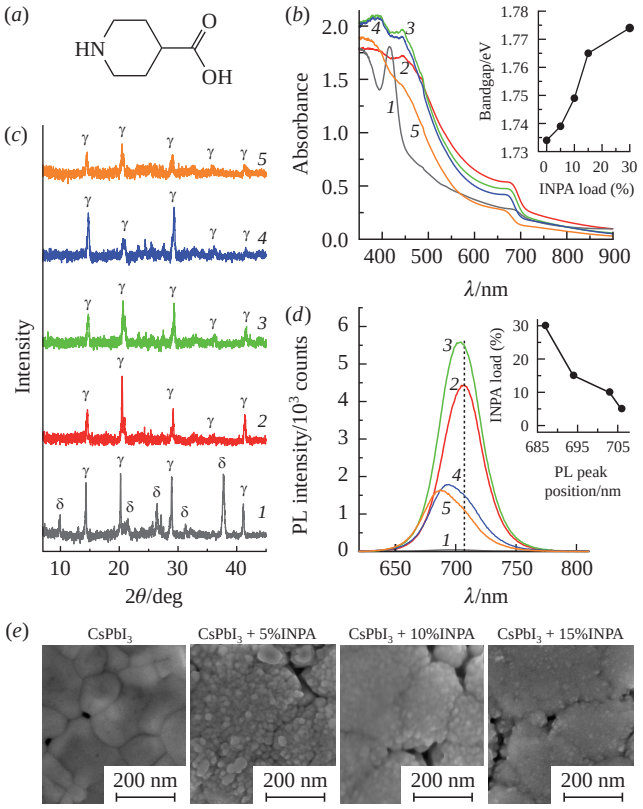

Figure 1 (*a*) Structural formula of INPA. Characterization of $CsPbI_3$ films, (*1*) pristine and loaded with (*2*) 5, (*3*) 10, (*4*) 15 and (*5*) 30% INPA: (*b*) UV-VIS absorption spectra (inset: dependence of bandgap value on INPA load), (*c*) XRD patterns, (*d*) PL spectra (inset: dependence of PL peak position on INPA load) and (*e*) SEM images.

optical absorption offsets were estimated for perovskite films from the Tauc plots (Figure S1, see Online Supplementary Materials), and the corresponding optical bandgap energies (E_g) are shown in the inset of Figure 1(*c*) and Table S1 (see Online Supplementary Materials). In the case of the pristine $CsPbI_3$ film, an absorption edge at 715 nm (bandgap of 1.734 eV) was observed in conjunction with a significantly reduced film absorbance in the 600–700 nm range. This decrease in absorbance is associated with a partial transition of the dark perovskite phase to the yellow one. The formation of the δ-$CsPbI_3$ phase is also indicated by an intense absorption peak at 450 nm, which is consistent with the results of XRD phase analysis [see Figure 1(*c*)]. The obtained E_g value was found to be close to the values reported in the literature for γ-$CsPbI_3$.[28]

All INPA-modified cesium lead triiodide films exhibited only the dark perovskite phase. A blue shift of the absorption edge is observed from 713 nm (1.739 eV) to 699 nm (1.774 eV) with increasing INPA concentration in $CsPbI_3$ films from 5 to 30%, respectively [Figure 1(*c*), inset].

As the INPA modifier content increased from 5 to 30%, a blue shift from 706 to 687 nm was also observed for the photoluminescence (PL) peak position [Figure 1(*d*), inset, and Table S2]. In addition, a noticeably higher PL intensity was observed for the modified absorber films with 10% INPA compared to the pristine $CsPbI_3$ films. Further increase in INPA loading resulted in a decrease in PL intensity.

The enhanced PL intensity can be attributed to the suppression of nonradiative carrier recombination as well as the reduction in the density of defects and charge traps in INPA-modified $CsPbI_3$ films, such as Cs^+ vacancies and undercoordinated Pb^{2+} formed in thin films of pristine $CsPbI_3$ during crystallization.[29,30]

Scanning electron microscopy (SEM) was used to explore the morphology of the thin films. Figures 1(*d*) and S2 show SEM

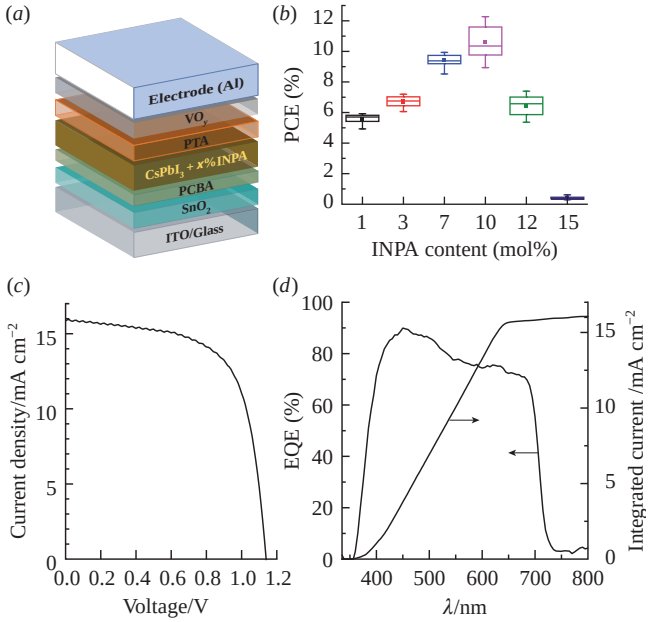

Figure 2 (*a*) Device structure, (*b*) evolution of solar cell efficiency values depending on the INPA content in $CsPbI_3$ films, (*c*) current–voltage characteristic and (*d*) EQE spectra of the best device based on $CsPbI_3$ + 10% INPA absorber films.

images, while Figure S3 features the grain size distribution for $CsPbI_3$ films with different INPA loadings. It is clearly seen that the introduction of the additive significantly suppresses the growth of crystals in perovskite films compared to the film of an unmodified absorber. The average grain size in pristine perovskite films reaches 250–300 nm, while as the INPA content increases from 5 to 30%, the grain size decreases from approximately 25 to 15 nm. These results are consistent with the XRD data, according to which the modified films demonstrate lower intensity of diffraction peaks, indicating a decrease in crystallinity [see Figure 1(*b*)].

To evaluate the effect of INPA modification on the photovoltaic performance of $CsPbI_3$ + *x*% INPA absorber films, devices with a planar configuration of n-i-p ITO/c-SnO_2/$CsPbI_3$ + *x*% INPA/PTA/VO_y/Al were fabricated [Figure 2(*a*)]. SnO_2 and PTA/VO_y were selected as materials for the electron transport layer and hole transport/electron blocking layers, respectively. The INPA content in the absorber films varied from 1 to 15 mol% (for details, see Online Supplementary Materials).

Figure 2(*b*) illustrates the evolution of solar cell PCE values as a function of INPA content in $CsPbI_3$ absorber films, while the photovoltaic parameters of the devices are summarized in Figure S3 and Table S2. The best photovoltaic parameters (PCE = 12.0%, open circuit voltage V_{OC} = 1135 mV, short circuit current density J_{SC} = 16.0 mA cm^{-2} and fill factor FF = 66%) were obtained by incorporating 10% INPA into the $CsPbI_3$ absorber layer, as can be seen from Figures 2(*b*), S4 and Table S3. The relevant photocurrent density–voltage (*J*–*V*) curves of the champion solar cells recorded under simulated AM1.5G illumination (100 mW cm^{-2}) are shown in Figure 2(*c*). The obtained short circuit current densities were reconfirmed by integrating the external quantum efficiency (EQE) spectra against the standard AM1.5G solar irradiation spectrum, as shown in Figure 2(*d*). An increase in the INPA content in the absorber layer beyond 10% results in a drop of all photovoltaic parameters, presumably, due to a deterioration of the charge transport properties of perovskite films [Figures 2(*b*), S4 and Table S2].

To identify the effect of modification with INPA on the phase photostability of $CsPbI_3$, the evolution of the optical properties and phase composition of pristine and modified perovskite films deposited on glass substrates was monitored under continuous light

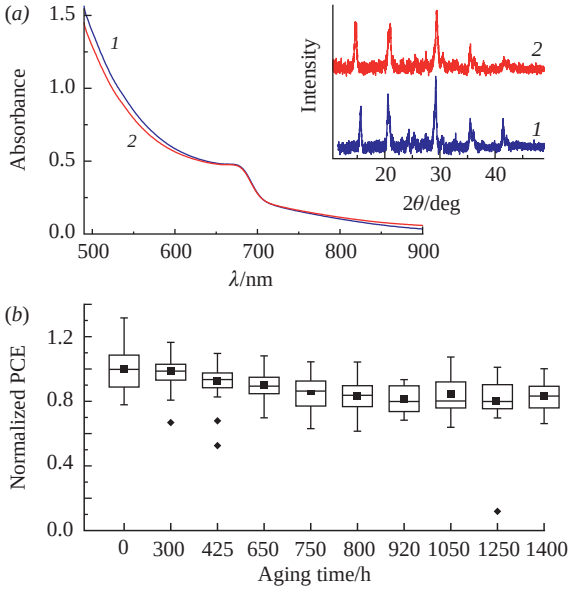

Figure 3 (*a*) UV-VIS absorption spectra and (inset) XRD patterns of as-prepared $CsPbI_3$ + 10% INPA films (*1*) before and (*2*) after continuous illumination with white light (500 mW cm^{-2} at 35 ± 2 °C) for 1500 h in an inert atmosphere. (*b*) Evolution of the normalized PCE of devices based on $CsPbI_3$ + 10% INPA absorber films during 1400 h of continuous light exposure under the same illumination conditions at open circuit.

illumination with an intensity of 500 ± 10 mW cm^{-2} at a temperature of 35 ± 2 °C for 1500 h in an inert atmosphere. The UV-VIS absorption spectra and XRD patterns of the $CsPbI_3$ + 10% INPA films before and after aging tests are shown in Figure 3(*a*). It can be observed that these films do not undergo any significant photobleaching, phase transition or other kind of decomposition upon continuous exposure to light for 1500 h [see Figure 3(*a*)]. On the contrary, the pristine $CsPbI_3$ films undergo a complete transition to the yellow δ-$CsPbI_3$ phase after 12 h under the same conditions (Figure S5).

The effect of the amount of loaded INPA on the operational stability of $CsPbI_3$-based perovskite solar cells was also explored under continuous light illumination (500 mW cm^{-2}, 35 ± 2 °C) in a nitrogen-filled glove box for 1400 h. Devices with 10% INPA in the absorber layer retained up to 80% of their initial efficiency [Figure 3(*b*)], while cells based on unmodified $CsPbI_3$ were completely degraded in just a few hours. The observed operational stability of INPA-modified devices is one of the best results ever reported for $CsPbI_3$-based perovskite solar cells.

The stabilizing effect of the INPA modifier can be explained by the presence in its molecular structure of amino and carboxyl groups, which are able to bind to undercoordinated surface Pb^{2+} cations and thereby passivate defects.[31,32] In addition, the introduction of INPA slows down the formation of perovskite films and drastically reduces the grain size in perovskite films, which makes the dark phase of $CsPbI_3$ more thermodynamically stable.[16]

In conclusion, we proposed isonipecotic acid as an efficient modifier to significantly improve the phase photostability of the well-known inorganic absorber material $CsPbI_3$ for perovskite solar cells. We found that optimal loading of 10% INPA in $CsPbI_3$ films suppresses the light-induced phase transition leading to a non-photoactive δ-phase. Furthermore, perovskite solar cells based on modified $CsPbI_3$ + 10% INPA films achieved a PCE of 12% and retained more than 80% of the initial PCE after 1400 h exposure to light (500 mW cm^{-2}, equivalent to 5 suns). The results presented in this work reveal a new strategy for using inorganic lead halide absorber materials to provide both high efficiency and long-term stability of perovskite solar cells.

This work was supported by the Ministry of Science and Higher Education of the Russian Federation [project no. 075-15-2022-1217 (13.2251.21.0163)].

Online Supplementary Materials

Supplementary data associated with this article can be found in the online version at doi: 10.1016/j.mencom.2024.06.004.

References

1 [dataset] NREL, *Best Research-Cell Efficiency Chart*, 2023, https://www.nrel.gov/pv/cell-efficiency.html.
2 H. Wang, Z. Dong, H. Liu, W. Li, L. Zhu and H. Chen, *Adv. Energy Mater.*, 2021, **11**, 2002940.
3 Y. Tu, G. Xu, X. Yang, Y. Zhang, Z. Li, R. Su, D. Luo, W. Yang, Y. Miao, R. Cai, L. Jiang, X. Du, Y. Yang, Q. Liu, Y. Gao, S. Zhao, W. Huang, Q. Gong and R. Zhu, *Sci. China: Phys., Mech. Astron.*, 2019, **62**, 974221.
4 L. Meng, J. You and Y. Yang, *Nat. Commun.*, 2018, **9**, 5265.
5 A. F. Akbulatov, S. Yu. Luchkin, L. A. Frolova, N. N. Dremova, K. L. Gerasimov, I. S. Zhidkov, D. V. Anokhin, E. Z. Kurmaev, K. J. Stevenson and P. A. Troshin, *J. Phys. Chem. Lett.*, 2017, **8**, 1211.
6 E. Mosconi, D. Meggiolaro, H. J. Snaith, S. D. Stranks and F. De Angelis, *Energy Environ. Sci.*, 2016, **9**, 3180.
7 G. E. Eperon, G. M. Paternò, R. J. Sutton, A. Zampetti, A. A. Haghighirad, F. Cacialli and H. J. Snaith, *J. Mater. Chem. A*, 2015, **3**, 19688.
8 J. Zhang, G. Hodes, Z. Jin and S. (F.) Liu, *Angew. Chem., Int. Ed.*, 2019, **58**, 15596.
9 H. Bian, D. Bai, Z. Jin, K. Wang, L. Liang, H. Wang, J. Zhang, Q. Wang and S. (F.) Liu, *Joule*, 2018, **2**, 1500.
10 A. Ho-Baillie, M. Zhang, C. F. J. Lau, F.-J. Ma and S. Huang, *Joule*, 2019, **3**, 938.
11 X. Zhang, Q. Wang, Z. Jin, J. Zhang and S. (F.) Liu, *Nanoscale*, 2017, **9**, 6278.
12 A. Shpatz Dayan, B.-E. Cohen, S. Aharon, C. Tenailleau, M. Wierzbowska and L. Etgar, *Chem. Mater.*, 2018, **30**, 8017.
13 Y. Jiang, J. Yuan, Y. Ni, J. Yang, Y. Wang, T. Jiu, M. Yuan and J. Chen, *Joule*, 2018, **2**, 1356.
14 T. Zhang, M. I. Dar, G. Li, F. Xu, N. Guo, M. Grätzel and Y. Zhao, *Sci. Adv.*, 2017, **3**, e1700841.
15 Q. Wang, X. Zheng, Y. Deng, J. Zhao, Z. Chen and J. Huang, *Joule*, 2017, **1**, 371.
16 Q. Wang, Z. Jin, D. Chen, D. Bai, H. Bian, J. Sun, G. Zhu, G. Wang and S. (F.) Liu, *Adv. Energy Mater.*, 2018, **8**, 1800007.
17 D. Jia, J. Chen, M. Yu, J. Liu, E. M. J. Johansson, A. Hagfeldt and X. Zhang, *Small*, 2020, **16**, 2001772.
18 X. Liu, X. Wang, T. Zhang, Y. Miao, Z. Qin, Y. Chen and Y. Zhao, *Angew. Chem., Int. Ed.*, 2021, **60**, 12351.
19 Y. Wang, X. Liu, T. Zhang, X. Wang, M. Kan, J. Shi and Y. Zhao, *Angew. Chem., Int. Ed.*, 2019, **58**, 16691.
20 J. Wang, S. Fu, X. Liu, H. Yuan, Z. Xu, C. Wang, J. Zhang, L. Huang, Z. Hu and Y. Zhu, *J. Alloys Compd.*, 2022, **891**, 161971.
21 Y. Wang, T. Zhang, M. Kan and Y. Zhao, *J. Am. Chem. Soc.*, 2018, **140**, 12345.
22 J. Huang, P. Xu, F. Yu, J. Liu, Y. Shirai, X.-P. Zhang, C.-H. Li and Y. Song, *J. Solid State Chem.*, 2023, **324**, 124087.
23 X. Ding, M. Cai, X. Liu, Y. Ding, X. Liu, Y. Wu, T. Hayat, A. Alsaedi and S. Dai, *ACS Appl. Mater. Interfaces*, 2019, **11**, 37720.
24 Y. Guo, H. Liu, W. Li, L. Zhu and H. Chen, *Sol. RRL*, 2020, **4**, 2000380.
25 Z. Qiu, N. Li, Z. Huang, Q. Chen and H. Zhou, *Small Methods*, 2020, **4**, 1900877.
26 R. Montecucco, E. Quadrivi, R. Po and G. Grancini, *Adv. Energy Mater.*, 2021, **11**, 2100672.
27 R. J. Sutton, M. R. Filip, A. A. Haghighirad, N. Sakai, B. Wenger, F. Giustino and H. J. Snaith, *ACS Energy Lett.*, 2018, **3**, 1787.
28 L. Duan, H. Zhang, M. Liu, M. Grätzel and J. Luo, *ACS Energy Lett.*, 2022, **7**, 2911.
29 Y. Huang, W.-J. Yin and Y. He, *J. Phys. Chem. C*, 2018, **122**, 1345.
30 Y.-H. Kye, C.-J. Yu, U.-G. Jong, K.-C. Ri, J.-S. Kim, S.-H. Choe, S.-N. Hong, S. Li, J. N. Wilson and A. Walsh, *J. Phys. Chem. C*, 2019, **123**, 9735.
31 M. M. Byranvand and M. Saliba, *Sol. RRL*, 2021, **5**, 2100295.
32 Y. Yin, Z. Guo, G. Chen, H. Zhang and W.-J. Yin, *Acta Phys.-Chim. Sin.*, 2021, **37**, 2008048.

Received: 23rd January 2024; Com. 24/7378